

## Solid-state seeded nano-second pulse CO<sub>2</sub> oscillator for extreme ultraviolet lithography

Krzysztof M. Nowak

*Gigaphoton Inc, 400 Yokokura Shinden, Oyama, 323-8558, Japan*

Received July 24, 2013; accepted September 26, 2013; published September 30, 2013

**Abstract**—This Letter describes in some detail a novel, solid-state seeded, nano-second pulse, multi-line CO<sub>2</sub> oscillator designed and built for the extreme ultraviolet (EUV) laser-produced-plasma (LPP) source. The oscillator employed quantum cascade laser (QCL) seeders, a spectral beam combiner and a diffusion-cooled, radio-frequency-discharge excited, slab-waveguide CO<sub>2</sub> amplifier in a multi-pass and compact regenerative amplifier configuration. The output spectrum consisted of individually controlled laser lines of 00°1-10°0 band of a CO<sub>2</sub> molecule, P18, P20 and P22 with a target 4-line operation (P18-P24). The resistance to self-oscillation of more than 40dB and to the external seeding of more than 55dB was realized. The oscillator produced up to 20W of average output power at repetition rate of 100kHz in a near-diffraction limited beam of  $M^2 < 1.3$  and RMS pointing stability below 50 microradians.

One of key elements in a shift towards a new generation of nanolithography, conceived to overcome a feature size limit imposed by the longer wavelength of currently used KrF and ArF excimer lasers, is the extreme ultraviolet (EUV) source. The 13.5nm wavelength targeted by the first generation of EUV lithography is obtained from tin plasmas driven by a pulsed electrical discharge (discharge-produced-plasma, DPP) or by pulsed high-power nanosecond CO<sub>2</sub> lasers (laser-produced-plasma, LPP). This combination of target material and the drive wavelength were chosen as a best compromise of achievable average drive power, the reflectivity of EUV optics, the availability of the resists, the EUV conversion efficiency, the minimum debris and the environmental safety. An interested Reader will find an excellent overview of the EUV technologies and history in Ref. [1].

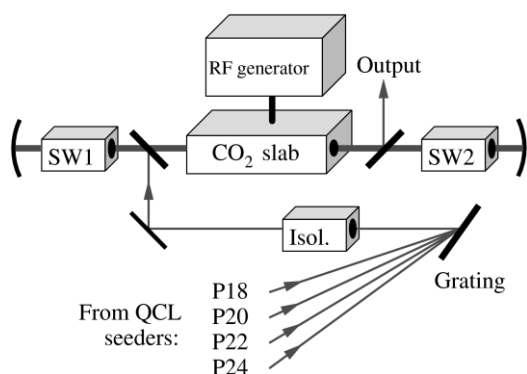


Fig. 1. Schematic view of the key components of the oscillator design.

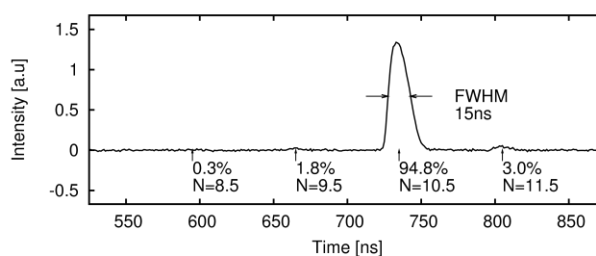


Fig. 2. A typical output pulse shape at single-line, QCL-seeded operation. Time counted from the instant of seed injection. Operation on P18 line at 100kHz pulse frequency, 10.5 round-trips. Energy fraction shown for the main pulse, pre- and post-pulses. Recorded using ~1ns rise time photovoltaic sensor PV-10.6 by Vigo SA.

The LPP EUV source requires the laser driver to produce short pulses of 5-20 nanosecond duration and repetition rates in excess of tens of kHz [2-3]. Such pulse format and repetition frequency are practically achievable by existing CO<sub>2</sub> technology only in a Master-Oscillator-Power-Amplifier (MOPA) scheme. An overview of relevant CO<sub>2</sub> technology and the state-of-the-art was given in Ref. [4]. This Letter focuses more on a key component of the MOPA system, the solid-state seeded nano-second pulse CO<sub>2</sub> laser [5] employing for the first time the quantum-cascade lasers as seeders [6-7].

A schematic of the laser is shown in Fig. 1 and a typical output pulse shape in Fig. 2. The construction of the laser is discussed here only briefly (a more detailed description was given in Ref. [5]) to devote more room to some interesting operational characteristics not described before. The beams of individually controlled QCL seeders were combined by means of a blazed grating (efficiency >60%), which also provided a broadband isolation function. Subsequently, the combined beam was relayed through an optical isolator onto the input of the regenerative amplifier. The two electro-optical switches, SW1 and SW2 controlled the timing of the input and output "time windows", determining the number of round-trips the input pulse would experience. A two-switch configuration was selected to physically separate the input and output planes and to relax speed requirements of the switches. The intentionally long round-trip time (~70ns) was achieved by employing a RF-discharge-excited,

diffusion-cooled, Cartesian slab-waveguide CO<sub>2</sub> amplifier module with a multi-pass optical configuration. The round-trip time longer than the input pulse duration eliminated the possibility of a regenerative-type feedback and a coupling of the input energy to the cavity eigenmodes. When combined with QCL seeding [6], such a configuration of the oscillator has got a number of unique features, such as an absence of the cavity eigenmodes, exceptional stability of the pulse envelope, possibility of a multi-line operation and a live pulse shape and duration adjustment, to name a few of them [5].

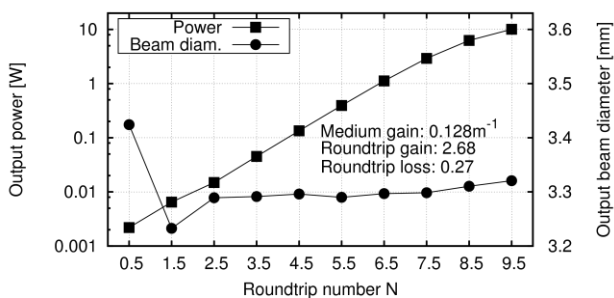


Fig. 3. Output power and output beam diameter of the oscillator measured as a function of round-trip number at 100kHz pulse frequency. About 1mW of average seed power in ~14ns pulses (P20 line) at 100kHz was provided from an attenuated EOM-10 laser in a near-collimated beam of about 3mm diameter. Output beam diameter (ISO D4 $\sigma$  method) is seen to stabilize already after a few round-trips.

The round-trip gain,  $G_r$ , and a number of round-trips,  $N$  constitute a basic parameter set describing the operation of this kind of oscillator. It was observed experimentally (see Fig. 3) that the power gain,  $G$  followed quite closely, up to a point of increasing saturation of the amplifying medium, the expected exponential characteristics described by Eq. (1):

$$G = \frac{P_o}{P_i} = G_r^N \quad (1)$$

The round-trip gain was also described rather well by Eq. (2):

$$G_r = T_r \exp(g_o L) \quad (2)$$

where  $T_r$  is a round-trip transmission (loss) and  $g_o L$  is a total gain-length product of one round-trip. The maximum  $g_o L$  was measured to be around 6, making it possible to achieve round-trip gain  $G_r > 100$  easily, and total power gain  $G > 10^6$  after just a few round-trips.

Such behaviour is indicative of a rapid stabilization of spatio-temporal characteristics of the input pulse, leading to a decoupling of the output beam parameters from the input beam characteristics and to a formation of well-defined output pulse shape. In fact, both aspects were observed experimentally.

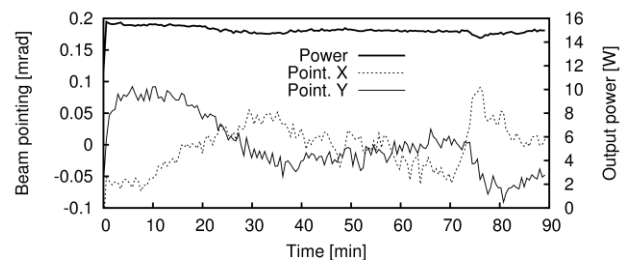


Fig. 4. ~50  $\mu$ rad RMS cold-start beam pointing stability in the free-space (X) and waveguide coordinate (Y) of the oscillator was measured using a  $f=1$ m lens and a Pyrocam camera located at the focal point. Free-run operation at 7.5 round-trips and 100kHz pulse frequency without any closed-loop control.

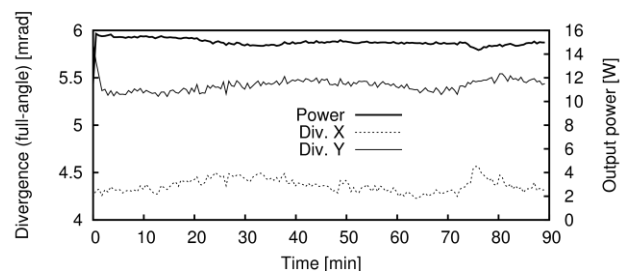


Fig. 5. Full-angle beam divergence in the free-space (X) and waveguide coordinate (Y) of the oscillator was measured using a  $f=1$ m lens and a Pyrocam camera located at the focal point. Free-run operation at 7.5 round-trips and 100kHz pulse frequency without any closed-loop control.

The rapid convergence of the output beam diameter is shown in Fig. 3. Only 2.5 round-trips were seen sufficient for the beam to converge to a final state, a result of an intentional design of the cavity implementing a rather strong (and lossy) optical beam filtering and shaping, made possible by the availability of large round-trip gain. The other advantage of high  $G_r$  was a mitigation of optical leakage of the switches and a reduction of the energy of parasitic pre- and post-pulses down to a tolerable level, as can be seen in Fig. 2. The optical filtering, achieved by a placement of appropriate apertures in the planes of the beam waists, was also believed responsible for a good stability of the beam in terms of pointing and divergence, as shown in Figs. 4 and 5. The pointing stability was mainly determined by changes of the coolant temperature and about 50 $\mu$ rad RMS beam pointing stability was recorded without any efforts at stabilization of either the coolant temperature or the beam itself. The value of  $T_r$  was measured to be ~0.27 from a knowledge of the  $g_o, L$  and the measured round-trip gain  $G_r$ . It was also confirmed that the farfield beam patterns were practically independent of the parameters (and quality) of the input beams, as can be seen in Fig. 6. Nearly identical farfield beam profiles were obtained with quite different input beams from the QCL lasers operating on P20 or P22 line or both simultaneously. The data in Fig. 5 indicated a beam propagation factor  $M^2 < 1.1$  in the free-space

coordinate (X) of the multi-pass amplifier and  $M^2 < 1.5$  in the coordinate across the waveguide (Y), resulting in a geometrical mean  $M^2 < 1.3$ . The optical filtering resulted therefore in a practically diffraction limited performance in the X coordinate with the Y coordinate being affected by an appreciably multi-modal propagation characteristics of the planar waveguide employed in the multi-pass amplifier.

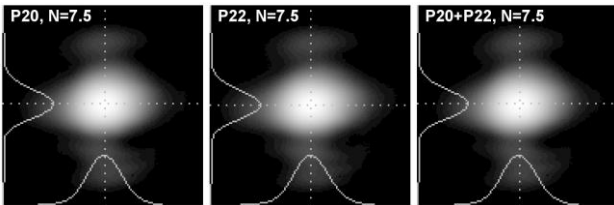


Fig. 6. Farfield profiles obtained with a  $f=1\text{m}$  lens and a Pyrocam camera located at the focal point. The images were prepared by mapping the logarithm of intensity to the levels of gray to visualize 20dB of dynamic range. Farfield profile was near-Gaussian and practically independent of the QCL input beam, be it either P20 or P22, or both. Free-run operation, 17.2W output power at 7.5 round-trips and 100kHz pulse frequency. Image size 12.4x12.4mm.

The availability of huge gain  $G$  made it possible to amplify the rather weak QCL energy, about 0.1-1 nJ per seeder, up to practical levels of  $>0.1\text{mJ}$  (at 100kHz pulse repetition that would be 10-100 $\mu\text{W}$  and  $>10\text{W}$  respectively). It was therefore reasonable to check whether it was possible to amplify such weak signals without the onset of cavity eigenmodes by determining the  $G_r$  and  $N$  necessary to obtain the same output target power but with the input signal originating from the spontaneous emission noise like in a conventional Q-switched  $\text{CO}_2$  laser. The result of such measurement is shown in Fig. 7 together with the computed  $G_r(N)$  curves (Eq.(1)) for a number of input power levels. The measurements have shown that the amplification from microWatt power levels was not a problem and a high self-oscillation suppression ratio  $S$  was feasible:

$$S = 10N \log \left( \frac{G_{r \text{ self}}}{G_r} \right) \quad [\text{dB}], \quad (3)$$

where  $G_{r \text{ self}}$  stands for the experimentally determined round-trip gain at given  $N$  in the self-oscillation mode of operation producing the same output power level as the seeded operation mode with round-trip gain  $G_r$  and the same  $N$ . The result of such calculation is shown in Fig. 8 showing that the QCL power quoted above was sufficient to provide the self-oscillation suppression in excess of 40dB, practically eliminating the cavity eigenmodes. As far as the external seeding by the back-propagating amplified stimulated emission (ASE) originating from the rest of MOPA system is concerned, the output switch SW2 can be configured as "normally closed", raising the resistance to the back-propagating light by 15dB to more

than 55dB, as compared to a conventional Q-switched  $\text{CO}_2$  laser, relaxing the requirement for the optical isolation significantly.

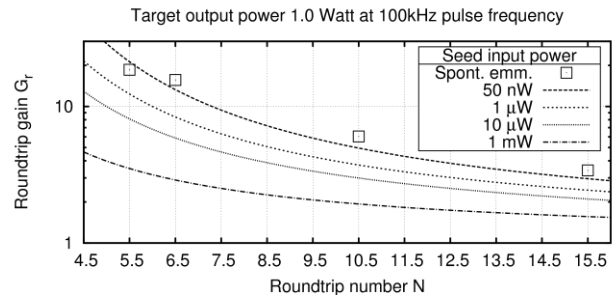


Fig. 7. A result of calculation of oscillator's control space (round-trip gain  $G_r$  and round-trip number  $N$ ) for a number of input seed power levels with a target output power level set below the saturation of the amplifier. The  $\{G_r, N\}$  required to amplify the internal spontaneous emission noise up to the target power level was determined experimentally and is plotted as well, indicating about 50nW of equivalent input power level.

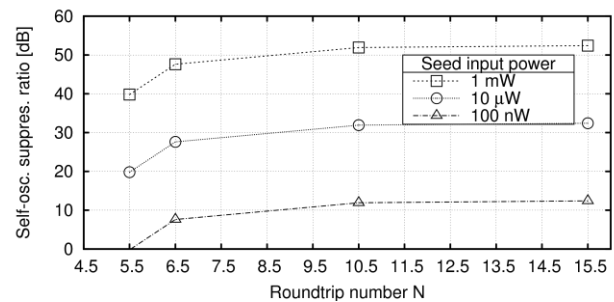


Fig. 8. The experimental data from Fig.7 were used to calculate the self-oscillation suppression ratio  $S$  for a number of input power levels. Over 40dB of self-oscillation suppression is achievable readily with a single QCL seed source.

Presently, a 4-line operation of the oscillator with P18, P20, P22 and P24 lines is being studied. The laser described in this Letter also has a potential for a range of applications such as precision high-speed laser material processing for example.

## References

- [1] V. Bakshi, *EUV lithography* (SPIE Press, 2009).
- [2] T. Ohta, K. M. Nowak, T. Sukanuma, H. Kameda, M. Moriya, T. Yokoduka, Y. Kawasuji, J. Fujimoto, H. Mizoguchi, *Proc. SPIE* **8322**, 832220 (2012).
- [3] D. C. Brandt, I.V. Fomenkov, M.J. Lercel, B.M. La Fontaine, D.W. Myers, D.J. Brown, *et al.* *Proc. SPIE* **8322**, 832246 (2012).
- [4] K.M. Nowak, T. Ohta, T. Sukanuma, J. Fujimoto, H. Mizoguchi, A. Sumitani, A. Endo, *Opto-Electron. Rev.* **21**, 52 (2013).
- [5] K.M. Nowak, T. Ohta, T. Sukanuma, J. Fujimoto, H. Mizoguchi, *Opt. Lett.* **38**, 881 (2013).
- [6] K.M. Nowak, T. Ohta, T. Sukanuma, T. Yokotsuka, J. Fujimoto, H. Mizoguchi, A. Endo, *Opt. Lett.* **37**, 4765 (2012).
- [7] K.M. Nowak, T. Ohta, T. Sukanuma, T. Yokotsuka, J. Fujimoto, H. Mizoguchi, *Opt. Lett.* **37**, 4886 (2012).